

## INFLUENCE OF CROSS-SECTIONAL CONFIGURATION ON KÁRMÁN VORTEX EXCITATION

MIZUYASU KOIDE

Life Engineering Research Center, Niigata Sangyo University  
4730 Karuigawa, Kashiwazaki, Niigata, 945-1393, Japan  
mkoide@life-eng.nsu.ac.jp

TSUTOMU TAKAHASHI, MASATAKA SHIRAKASHI

Department of Mechanical Engineering, Nagaoka University of Technology  
1603-1 Kamitomioka, Nagaoka, Niigata, 940-2188, Japan

[Received: November 12, 2003]

**Abstract.** Three cylindrical bodies with different cross-sectional configurations, i.e. a circular, semi-circular and triangular cylinder, are used as the test cylinders, in order to investigate the influence of movement of the separation point on the Kármán vortex excitation. The cylinders were supported elastically by plate springs. The synchronization of Kármán vortex shedding occurs on all three cylinders over almost equal ranges of oscillation amplitude and frequency given by the mechanical oscillator. However, the Kármán vortex excitation behavior differs drastically among the three cylinders in spite of the fact that the cylinders are supported elastically with virtually equal structure parameters.

*Mathematical Subject Classification:* 76B47, 76D25

*Keywords:* Kármán vortex excitation, cross-sectional configuration, synchronization

### 1. Introduction

The Kármán vortex excitation is an oscillation caused by the hydrodynamic force which originates from periodic Kármán vortex formation and shedding, and it has basically the nature of resonance of a linear system. That is, the cylinder is oscillated by the alternating force due to Kármán vortex shedding and the amplitude is large when the vortex shedding frequency  $f_v$  is equal to the natural frequency of the structure  $f_n$ . The cylinder motion affects the flow around it and then the magnitude and frequency of exciting force in turn.

Therefore, the Kármán vortex excitation is regarded as non-linear self-excitation caused by the feedback loop which is constituted by two interactions, i.e. the effect of cylinder motion on the fluid force due to the periodic vortex shedding and the response of the structure to the resulting fluid force. Hence, its mechanism can be discussed by separating the process into the two interactions.

Funakawa [1] showed that the separation point on an oscillating circular cylinder moves forward and backward, synchronized with the cross-flow oscillation. Based

on this observation he suggested a self-excitation mechanism for the Kármán vortex excitation.

In this work, influence of the cross-sectional configuration of a cylindrical body on the Kármán vortex excitation was investigated experimentally by using a circular cylinder, a semi-circular cylinder and a triangular cylinder, in order to investigate the role of separation point movement in the mechanism of the Kármán vortex excitation.

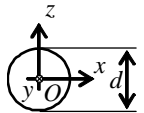
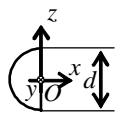
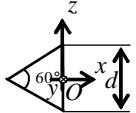
## 2. Experimental apparatus and measurements

Table 1 shows cross-sectional configurations of the cylinders used in this investigation. They were set in a uniform flow from left to right (in the  $x$ -direction) in a wind tunnel. When the cylinders are set in a uniform flow, the separation point movement is free on the circular cylinder surface, restricted to the upstream circular arc of the semi-circular cylinder and fixed at the downstream vertices of the triangular cylinder [2]. Measurements were carried out in a blow-down type wind tunnel with a measuring section of  $320 (H) \times 320 (W) \times 1000 (L) \text{ mm}$ . The turbulence level at the center of the measuring section is less than 0.6 % at  $U = 2.0 \text{ m/s}$ . A ring type vortex anemometer [3] was applied to measure  $U$ .

Figure 1 shows the experimental apparatus arrangement for the measuring section. The test cylinder was set horizontally and perpendicularly to the free stream. The height  $d$  of each cylinder was  $26 \text{ mm}$  and the blocking ratio was about 8 %. The cylinder was passing through slots on the side walls and supported at both ends outside the measuring section, as shown in Figure 1. End plates were attached to the cylinder to remove influence of flow through the slots [4].

The elastically supported system is composed of two cantilever plate springs. Since the length of the cantilever plate is much longer than the oscillation amplitude  $A$ , the cylinder motion is regarded as translational oscillation in the vertical direction ( $z$ -direction), i.e. cross-flow oscillation. Two laser displacement meters were used to measure cylinder displacement  $Z$  at both ends of the cylinder, as shown in Figure 1. The oscillation amplitude  $A$  was calculated from root-mean square (rms) value of  $Z$ , i.e.  $A = \sqrt{2}Z_{rms}$ .

Table 1. Cross-sectional configuration and effective mass  $m_e$  of the elastically supported cylinders ( $d = 26 \times 10^{-3} \text{ m}$ )

	Circular cylinder	Semi-circular cylinder	Triangular cylinder
Effective Mass [kg]	$53.7 \times 10^{-3}$	$50.1 \times 10^{-3}$	$50.7 \times 10^{-3}$
Cross-sectional Configuration			
Flow direction: from left to right			

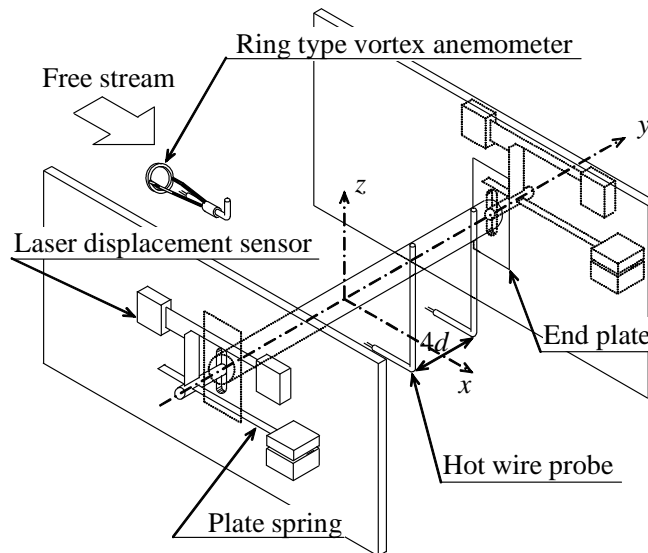


Figure 1. Arrangement of the experimental apparatus (elastically-supported system) and the coordinate system

The natural frequency  $f_n$ , effective mass  $m_e$  and logarithmic damping factor  $\delta$  of the system were determined by free damping oscillation in otherwise quiescent air. The values of  $f_n$ ,  $m_e$  and  $\delta$  were set virtually equal for all the three cylinders.

The vortex shedding frequency  $f_v$  was obtained by applying FFT analysis to the streamwise fluctuating velocity  $u$  detected by a hot wire probe at a location in the near wake of the cylinder ( $x = 2d$ ,  $z = d$ ). The spectrum of  $u$  was averaged over 20 data to reduce the effect of turbulence. The vortex shedding frequency  $f_v$  was determined as the frequency at which the spectrum of  $u$  had the maximum peak. Furthermore, the phase difference between  $u$  and  $Z$  was calculated and its average value  $\phi_{uZ}$  was obtained from 20 data. The standard deviation of  $\phi_{uZ}$ ,  $\sigma_\phi$  was also obtained. The cross-correlation coefficient  $R_{uu}$  was obtained from two  $u$  signals detected by two hot wire probes set with  $4d$  spanwise separation. The cross-correlation coefficient  $R_{uu}$  increases due to Kármán vortex excitation since it shows an enhancement of spanwise coherency of the Kármán vortex [2]. In this paper, the increase of  $R_{uu}$  is adopted as one of criteria to decide whether Kármán vortex excitation occurs or not.

The lift force  $F_L$  exerted on the stationary cylinder was measured by load transducers at both ends of the cylinder outside the measuring section.

### 3. Results and discussion

**3.1. Behavior of the cylinder oscillation and vortex shedding in Kármán vortex excitation.** Figures 2, 3 and 4 show the behavior of the cylinder oscillation

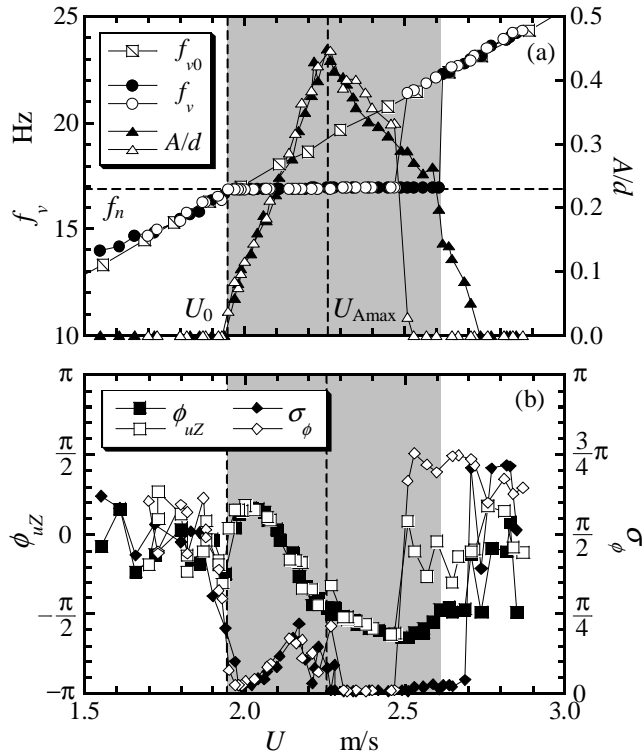


Figure 2.  $f_v$ ,  $A/d$ ,  $\phi_{uZ}$  and  $\sigma_\phi$  versus  $U$  for the circular cylinder.  $f_n = 16.93$  Hz,  $\delta = 0.00958$  (Closed symbols:  $U$  increased, open symbols:  $U$  decreased)

and vortex shedding against the free stream velocity  $U$  for the circular cylinder, the semi-circular cylinder and the triangular cylinder, respectively. In one run of the wind tunnel experiment,  $U$  was first increased stepwise from the lowest value of around  $1.5$  m/s to the velocity beyond the Kármán vortex excitation range, and then decreased again to the lowest velocity. The closed symbols are for increasing  $U$  and the open symbols for decreasing  $U$ , respectively.

The vortex shedding frequency  $f_v$  and the non-dimensional oscillation amplitude  $A/d$  are plotted in Figures 2(a), 3(a) and 4(a). The Kármán vortex shedding frequency from the stationary cylinder  $f_{v0}$  is also plotted to compare with  $f_v$ . In these Figures,  $U_0$  is the velocity at which  $f_{v0}$  coincides with the natural frequency of the system  $f_n$ , and  $U_{Amax}$  indicates the velocity at which  $A/d$  is maximum. Figures 2(b), 3(b) and 4(b) show the phase difference  $\phi_{uZ}$  between velocity fluctuation  $u$  and the cylinder displacement  $Z$  and its standard deviation  $\sigma_\phi$ . The shaded region is the Kármán vortex excitation region when  $U$  is increased.

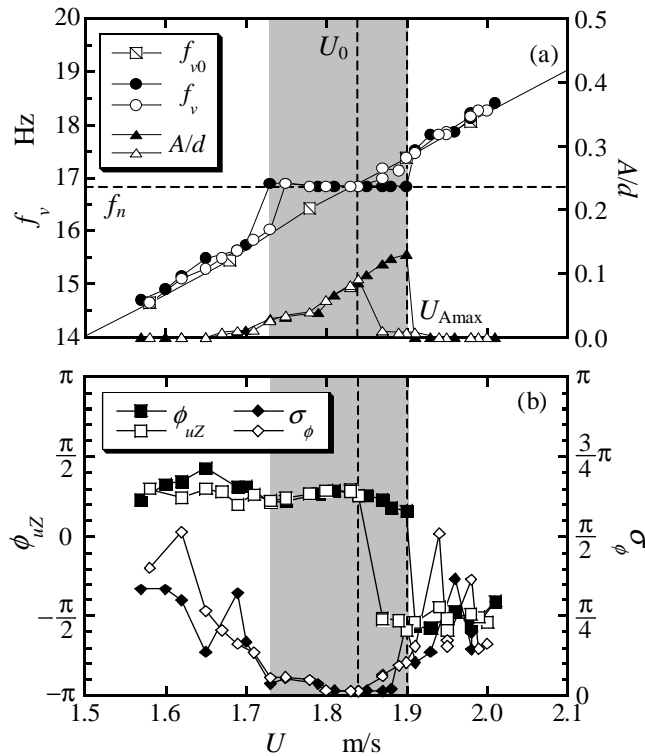


Figure 3.  $f_v$ ,  $A/d$ ,  $\phi_{uZ}$  and  $\sigma_\phi$  versus  $U$  for the semi-circular cylinder.  $f_n = 16.86$  Hz,  $\delta = 0.0116$  (Closed symbols:  $U$  increased, open symbols:  $U$  decreased)

3.1.1. *Circular cylinder.* Figure 2 shows the results of the circular cylinder. As shown in Figure 2(a), the oscillation amplitude  $A/d$  is large and the vortex shedding frequency  $f_v$  coincides with  $f_n$  over a certain velocity range including  $U_0$ , showing that the Kármán vortex excitation occurs there. In the case of the circular cylinder, the velocity  $U_0$  is very close to the lower velocity edge of the Kármán vortex excitation range. In contrast, the synchronization of Kármán vortex shedding was observed at both sides of  $U_0$  when the circular cylinder was oscillated with a certain amplitude and frequency using a mechanical oscillator [2].

The amplitude of the circular cylinder due to the Kármán vortex excitation has a maximum value of  $A/d = 0.4$  at  $U_{Amax}$ , which is considerably larger than  $U_0$ . In a linear oscillation model, the oscillation amplitude reaches its maximum when the frequency of the excitation force coincides with the natural frequency, which means that  $A/d$  would be maximum at  $U_0$  in the present experiment. From the discrepancy between  $U_0$  and  $U_{Amax}$ , it is inferred that the alternating lift force  $F_L$  exerted on

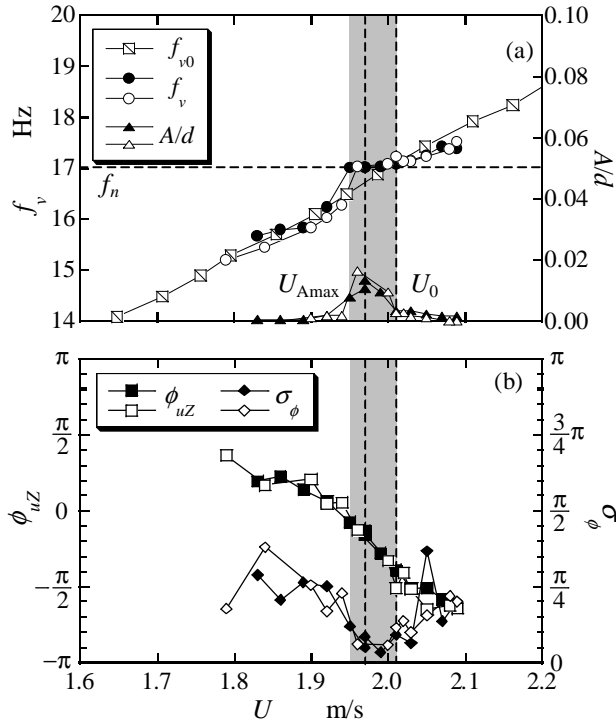


Figure 4.  $f_v$ ,  $A/d$ ,  $\phi_{uZ}$  and  $\sigma_\phi$  versus  $U$  for the triangular cylinder.  $f_n = 17.03 \text{ Hz}$ ,  $\delta = 0.0141$  (Closed symbols:  $U$  increased, open symbols:  $U$  decreased)

the oscillating cylinder is larger than that on the stationary cylinder and enhanced with the oscillation amplitude due to the influence of the cylinder oscillation on the Kármán vortex shedding.

A remarkable hysteresis is observed near the higher velocity edge of the excitation range, where both  $A/d$  and  $f_v$  at a same value of  $U$  differs depending on whether  $U$  is increased or decreased. When the circular cylinder was oscillated using a mechanical oscillator, such hysteresis was not observed. The phase difference  $\phi_{uZ}$  changes gradually in the excitation range around  $U_{Amax}$ , and the total amount of the change is approximately  $\pi$ , as seen in Figure 2(b). This shows that the timing of the vortex shedding becomes anti-phase against the cylinder oscillation. The standard deviation  $\sigma_\phi$  represents the extent of disturbance in  $\phi_{uZ}$ , and it is an index of coherency between the cylinder oscillation and the vortex shedding. In Figure 2(b),  $\phi_{uZ}$  varies continuously in the range  $U_0 < U < U_{Amax}$ , and  $\sigma_\phi$  considerably increases at the same time. This result shows that the coherency of vortex shedding with the cylinder

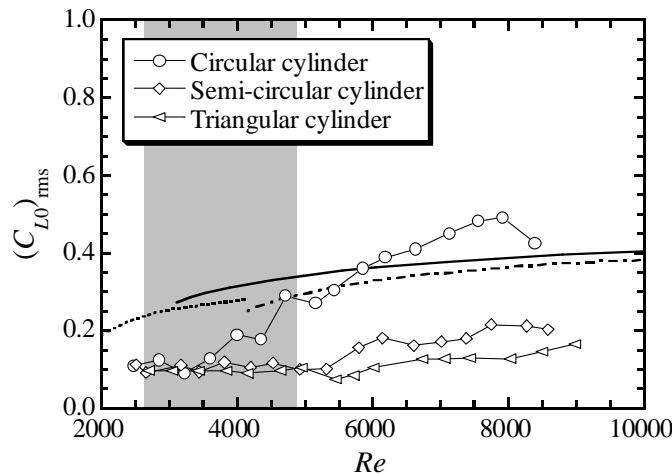


Figure 5. Lift coefficient on stationary cylinder  $(C_{L0})_{rms}$  versus Reynolds number  $Re$ . —··— Vickery; — Bishop and Hassan; —·— Keefe; for circular cylinder [5]. The shaded region shows the range of Kármán vortex excitation experiments for circular cylinder

oscillation becomes lower with  $U$  in this range. In contrast,  $\phi_{uZ}$  is nearly constant and  $\sigma_\phi$  is almost suppressed in the range of  $U > U_{Amax}$  in the excitation range, showing that the vortex shedding is completely synchronized with the cylinder oscillation.

**3.1.2. Semi-circular cylinder.** The Kármán vortex excitation occurs over a considerable velocity range in the case of the semi-circular cylinder as seen in Figure 3. However, the maximum amplitude for the semi-circular cylinder is 1/3 of that for the circular cylinder, in spite of the fact that the height  $d$ , the effective mass  $m_e$ , the logarithmic damping factor  $\delta$  and velocity  $U$  are almost the same in the two cases. When  $U$  increases, the non-dimensional amplitude  $A/d$  continues increasing in the excitation range, and the oscillation suddenly ceases soon after  $A/d$  reaches its maximum. The excitation range of the semi-circular cylinder lies on both sides of  $U_0$ , while that of the circular cylinder exists only on  $U \geq U_0$ .

A definite hysteresis is observed for the semi-circular cylinder in  $f_v$  and  $A/d \sim U$  curves at higher velocity edge of the excitation range, and the repeatability of the hysteresis behavior is much higher for the semi-circular cylinder than for the circular cylinder.

In the excitation range,  $\phi_{uZ}$  is virtually constant and  $\sigma_\phi$  is very small, showing that the vortex shedding is well synchronized with the cylinder oscillation. A sudden change of  $\phi_{uZ}$  is observed simultaneously with the cessation of the oscillation at the higher velocity edge. However, it cannot be concluded whether this change of  $\phi_{uZ}$  is caused by the same phenomenon that caused the change of  $\phi_{uZ}$  in the excitation range of the circular cylinder.

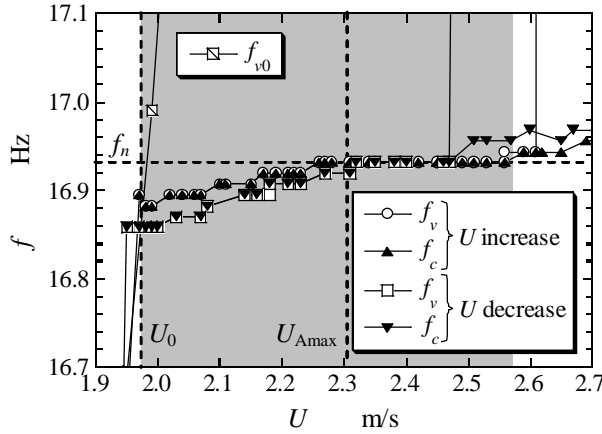


Figure 6. The details of vortex shedding frequency  $f_v$  and oscillation frequency  $f_c$  of the circular cylinder in Kármán vortex excitation region

3.1.3. *Triangular cylinder.* Although experimental conditions for the triangular cylinder are the same as those of the circular cylinder and the semi-circular cylinder, the maximum value of  $A/d$  is  $1/30$  of the circular cylinder as shown in Figure 4(a). The vortex excitation is observed over a narrow velocity range. It seems that the vortex excitation range lies on  $U \leq U_0$  in contrast to the cases of the circular and the semi-circular cylinders. The hysteresis is not discerned clearly, maybe because  $A/d$  is small and the vortex excitation range is narrow.

Figure 4(b) shows that  $\phi_{uZ}$  steeply decreases with  $U$  in the vortex excitation range. However, the standard deviation  $\sigma_\phi$  in Figure 4(b) is small over the same range, which indicates the occurrence of definite synchronization of Kármán vortex shedding in spite of the large change in  $\phi_{uZ}$ .

## 3.2. Lift force acting on the cylinder.

3.2.1. *Lift force acting on the stationary cylinder.* The alternating lift force  $F_L$ , which acts on the fixed cylinders, was measured over a free stream velocity  $U$  range including the vortex excitation range presented in Section 3.1. Since  $F_L$  was composed of the contributions of Kármán vortex shedding and other unsteady turbulence, the root mean square value of  $F_L$ ,  $(F_L)_{rms}$ , was used to estimate the magnitude of  $F_L$ . Hence, the fluctuating lift coefficient of a stationary cylinder  $(C_{L0})_{rms}$  was calculated by the following equation:

$$(C_{L0})_{rms} = \frac{(F_L)_{rms}}{\frac{1}{2}\rho U^2 dl}, \quad (3.1)$$

where  $\rho$  is air density,  $d$  is the height of the cylinder and  $l$  is the effective length of the cylinder defined as the distance between the two end plates (see Figure 1).



The lift coefficients  $(C_{L0})_{rms}$  for the three cylinders were plotted against the Reynolds number  $Re$  in Figure 5. The shaded region shows the range where the oscillation measurement for the circular cylinder was carried out.  $(C_{L0})_{rms}$  for a circular cylinder measured by Vickery, Bishop and Hassan, Keefe [5] was also plotted in Figure 5 for comparison. The lift coefficient  $(C_{L0})_{rms}$  of the circular cylinder obtained in this work agrees well with those by others when  $Re > 5000$ , but is considerably lower when  $2500 < Re < 4500$ .

The lift coefficient  $(C_{L0})_{rms}$  of the circular cylinder increases gradually with  $Re$  in the range of the oscillation experiment, say from 0.1 at  $Re = 2500$  to 0.3 at  $Re = 5000$ . While  $(C_{L0})_{rms}$  for the semi-circular cylinder and the triangular cylinder are equal to that of the circular cylinder when  $Re = 2500$ , they remain constant in the same  $Re$  range. Hence,  $(C_{L0})_{rms}$  of the circular cylinder is larger than those of the other two cylinders by a factor of 3 at  $Re = 5000$ .

### 3.2.2. Lift force acting on the oscillating cylinder excited by Kármán vortex excitation.

In order to estimate the alternating fluid force exerted on the cylinder under the Kármán vortex excitation, it is assumed that the cylinder supported elastically by two plate springs is a linear system with constant mass, spring and damping. Based on this assumption, the following equation determines the cylinder motion  $Z$

$$m_e \ddot{Z} + c\dot{Z} + kZ = F_L, \quad (3.2)$$

where  $m_e$  is the effective mass of the cylinder,  $c$  is the damping factor and  $k$  is the spring constant.  $F_L$  is the lift force caused by the periodic Kármán vortex shedding, and is assumed to be sinusoidal. That is,

$$F_L = F_0 \sin(2\pi f_v t). \quad (3.3)$$

From the solutions of equations (3.2) and (3.3) together with the definition of the lift coefficient  $(C_{LR})_{rms}$  as equation (3.1), we obtain

$$(C_{LR})_{rms} = \frac{8\pi^2 m_e f_n^2 A \sqrt{(1-\eta^2)^2 + (2\zeta\eta)^2}}{\sqrt{2}\rho U^2 dl}, \quad (3.4)$$

where  $\eta = f_v/f_n$  and  $\zeta$  is the damping ratio ( $= \delta/(2\pi)$ ). From equation (3.4) it is seen that a slight difference between  $f_v$  and  $f_n$  in the vortex excitation range affects  $(C_{LR})_{rms}$  drastically when the damping ratio  $\zeta$  is very small like in the experiments in this work. Therefore, the results for the circular cylinder in Figure 2(a) were examined more precisely. Figure 6 shows the oscillation frequency  $f_c$  and the vortex shedding frequency  $f_v$  in the vortex excitation range in detail. In this Figure, it is seen that  $f_c$  coincides with  $f_v$  but they do not coincide with  $f_n$  when  $U$  is smaller than  $U_{Amax}$ . The slight difference between  $f_v$  and  $f_c$  reflects the large value of  $\sigma_\phi$  in the range  $U_0 < U < U_{Amax}$  shown in Figure 2(b). When  $U > U_{Amax}$  in the vortex excitation range,  $f_c$  and  $f_v$  are strictly equal to  $f_n$ .

$(C_{LR})_{rms}$  was calculated using equation (3.4), based on the results that are described in Section 3.1. In Figure 7,  $(C_{LR})_{rms}$  of the circular cylinder, the semi-circular cylinder and the triangular cylinder are plotted against  $A/d$  for the cases of increasing  $U$ . In the Figure, the arrows indicate the order of measurement. The alternating

lift coefficients of the oscillating circular cylinder by Khalak and Williamson [6] and Hayashi et al. [7] are added for comparison. The former was measured directly in water and the latter in air.

The lift coefficient  $(C_{LR})_{rms}$  of the circular cylinder and the semi-circular cylinder are equal to each other and increase with  $A/d$  when  $A/d < 0.13$ . However, the maximum value of  $(C_{LR})_{rms}$  of the semi-circular cylinder is around 0.4 at  $A/d = 0.13$  while  $(C_{LR})_{rms}$  of the circular cylinder continues to increase till it attains the maximum value around unity, at  $A/d = 0.45$ . The lift coefficient  $(C_{LR})_{rms}$  of the triangular cylinder at very small amplitude is nearly equal to that of the other two cylinders, and no definite increase is observed since the range of  $A/d$  is limited. Although the experimental conditions for the three cylinders are almost the same, the maximum value of  $(C_{LR})_{rms}$  is quite different among them, e.g. maximum value of  $(C_{LR})_{rms}$  for the circular cylinder is about 10 times that for the triangular cylinder.

The difference between  $(C_{LR})_{rms}$  of the three cylinders with different cross-sectional configurations is attributed to the separation point movement of these cylinders [2]. For the circular cylinder, the separation point moves widely on the arc of surface synchronized with the cylinder oscillation. In contrast, the separation point on the triangular cylinder is fixed at the rear vertex irrespective of the cylinder oscillation.

The lift coefficient  $(C_{LR})_{rms}$  of the circular cylinder based on the linear analysis in this work coincides with the direct measurements by Khalak et al. [6] and Hayashi et al. [7] in the range of  $A/d < 0.13$ . When  $0.13 < A/d < 0.45$ ,  $(C_{LR})_{rms}$  of the higher stem (i.e.  $U < U_{Amax}$ ) in this work agrees well with that by Khalak et al., while that by Hayashi et al. is considerably higher. When  $A/d$  is still higher, or begins to decrease passing its maximum, results of the three works are largely different from each other. This may be because of the fact that the assumption of a linear model does not hold when  $A/d$  is large, or because of the difference between experimental conditions and ways of measurements.

**3.3. Occurrence region of the Kármán vortex excitation.** The synchronization region of the Kármán vortex shedding was investigated for all the three cylinders by giving them a controlled oscillation using a mechanical oscillator by the present authors [2]. Since the behavior of Kármán vortex excitation is disturbed by irregular modulation and its magnitude is drastically different among the three cylinders, the criterion of Kármán vortex excitation should be defined more precisely. According to the earlier study, occurrence of the Kármán vortex excitation is defined by a criterion composed of the following four conditions:

- i) an increase of the oscillation amplitude,
- ii)  $f_c = f_v$ ,
- iii) an increase of the cross-correlation coefficient  $R_{uZ}$  between the velocity  $u$  and the cylinder displacement  $Z$ , and
- iv) an increase of the cross-correlation coefficient  $R_{uu}$ .

When all of these four conditions are satisfied, the Kármán vortex excitation, and

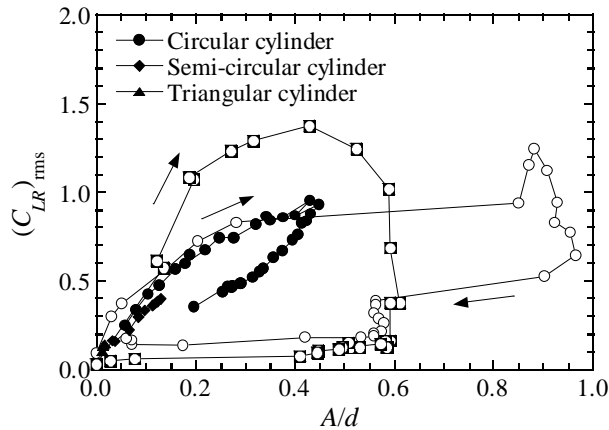


Figure 7. Lift coefficient  $C_{LR}$  for oscillating cylinder versus non-dimensional oscillation amplitude  $A/d$  under Kármán vortex excitation, when  $U$  increases.  $\circ$ —, Khalak and Williamson [6],  $\square$ —, K. Hayashi et al. [7], for circular cylinder

and hence the synchronization of vortex shedding with the cylinder oscillation, i.e. ‘Lock-in’, is decided to occur. When none of the four conditions are satisfied, it is taken to be no vortex excitation and ‘No Lock-in’. The remaining cases are defined as ‘Transition’.

The occurrence regions of the Kármán vortex excitation on the plane of frequency ratio  $f_{v0}/f_n$  and the non-dimensional amplitude  $A/d$  are plotted in Figures 8(a), 8(b) and 8(c) for each of the cylinders, where the synchronization data obtained by the controlled oscillation experiment are also added [2]. In these controlled oscillation experiments,  $Re$  was fixed at about 3500, i.e.  $U$  was constant at  $2\text{ m/s}$ , to exclude the influence of  $Re$ . Since the measurement of Kármán vortex excitation was carried out for increasing or decreasing  $U$ ,  $Re$  is not constant in these Figures. Some of the data were obtained by using systems with different damping factors.

As seen by comparing Figures 8(a), (b) and (c), the Kármán vortex excitation regions for the elastically supported cylinder are drastically different among them, although the synchronization regions for a controlled oscillation experiment are almost the same for all of the cylinders. The Kármán vortex excitation region for the semi-circular cylinder and the triangular cylinder lies within the synchronization region of controlled oscillation experiment. The Kármán vortex excitation region for the circular cylinder is the broadest among the three cylinders and exceeds beyond the lock-in region of controlled oscillation experiment when  $f_{v0}/f_n > 1$ . The following can be considered the causes for the discrepancy:

- i)  $Re$  was not kept constant for the vortex excitation experiment different from the controlled oscillation experiments,

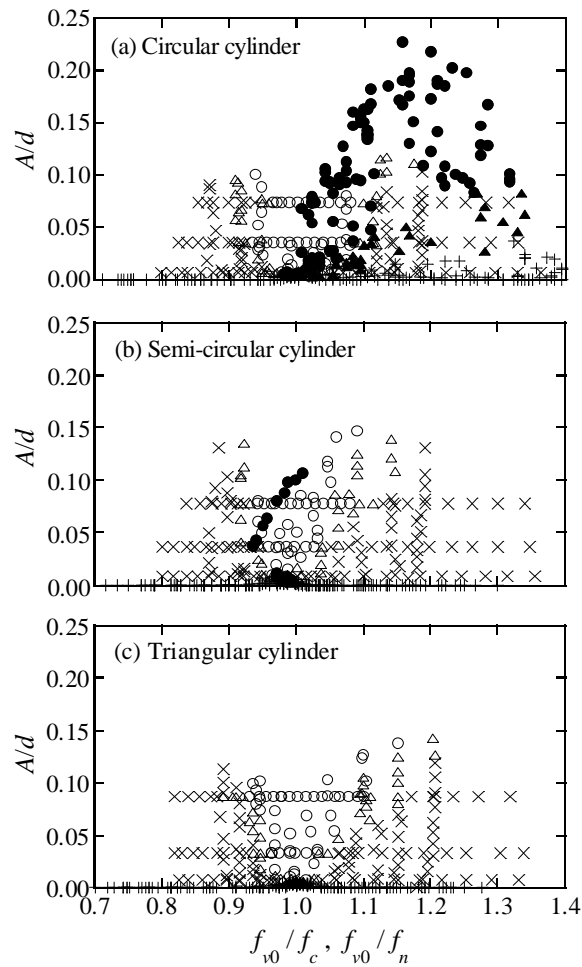


Figure 8. Kármán vortex excitation region on a plane of frequency ratio and non-dimensional amplitude. ● : Kármán vortex excitation, +: No excitation, ▲: Transition; Controlled oscillation, ○: Lock-in, ×: No Lock-in, △: Transition. [2]

- ii) the mechanical oscillator gives the cylinder a precise sinusoidal oscillation, while the Kármán vortex excitation includes considerable modulation of amplitude,
- iii) the cantilever support system induces an attack angle fluctuation synchronized with the cylinder oscillation superimposed on the  $z$ -displacement oscillation.

#### 4. Concluding remarks

In the previous work by the present authors the synchronization of Kármán vortex shedding was investigated by giving a controlled cross-flow oscillation to a circular, a semi-circular and a triangular cylinder, and it is shown that the synchronization region is almost the same for the three cylinders in spite of the different behaviors of separation point movement [2].

In this work, influence of the cross-sectional configuration of a cylindrical body on the Kármán vortex excitation was investigated experimentally by using the same cylinders to investigate the role of separation point movement in the Kármán vortex excitation. The three cylinders were supported elastically by cantilever plate springs so that the experimental conditions, such as the mass, natural frequency and damping factor, were almost equal.

Kármán vortex excitation appears on all the three cylinders. However, the oscillation behavior was drastically different among them.

The alternating lift coefficient is equal for the three cylinders when they are at rest. However, the lift coefficient  $(C_{LR})_{rms}$  obtained from measured oscillation amplitude  $A/d$  are largely different from each other. Although  $(C_{LR})_{rms}$  increases with  $A/d$  for all the three cylinders, the maximum value is largely different in each case, that is,  $(C_{LR})_{rms}$  is around 1.0 at  $A/d = 0.45$  for the circular cylinder, 0.4 at  $A/d = 0.15$  for the semi-circular cylinder and 0.1 at  $A/d = 0.05$ , for the triangular cylinder. This tendency of enhancement of lift coefficient by the oscillation corresponds with the separation point movement on these cylinders shown by the controlled oscillation experiment in the previous work.

In conclusion, the mechanism of the Kármán vortex excitation can be explained as follows. A cylinder is oscillated by the alternating lift force due to the periodic Kármán vortex shedding, and the amplitude reaches its maximum when the flow velocity is around  $U_0$ . The resulting cylinder oscillation causes the synchronization of the vortex shedding, which makes the resonance range of flow velocity broader than otherwise. At the same time, the cylinder oscillation influences the movement of the separation point and enhances the lift, depending on the cross-sectional configuration. This enhancement effect is largest for the circular cylinder and negligibly small for the triangular cylinder.

#### REFERENCES

1. FUNAKAWA, M.: Excitation mechanism of elastically supported circular cylinder in the flow. *Bulletin of the Japan Society of Mechanical Engineers*, **36**(285), (1970), 337-356. (in Japanese)
2. KOIDE, M., TOMIDA, S., TAKAHASHI, T., BARANYI, L. AND SHIRAKASHI, M.: Influence of cross-sectional configuration on the synchronization of Kármán vortex shedding with the cylinder oscillation. *Japan Society of Mechanical Engineers, International Journal*, **45**(2), (2002), 249-258.

3. KOIDE, M., TAKAHASHI, T. AND SHIRAKASHI, M.: Development of a ring-type vortex anemometer for low-velocity wind tunnel experiments. *Bulletin of Japan Society of Mechanical Engineers*, **7**(657), (2001), 1105-1111. (in Japanese)
4. SHIRAKASHI, M., ISHIDA, Y. AND WAKIYA, S.: Higher velocity resonance of circular cylinder in cross flow. *Transaction of the ASME Journal of Fluids Engineering*, **107**, (1985), 392-396.
5. GARTSHORE, I. S.: Some effects of upstream turbulence on the unsteady lift forces imposed on prismatic two dimensional bodies. *Journal of Fluids Engineering*, **106**, (1984), 418-424.
6. KHALAK, A. AND WILLIAMSON, C. H. K.: Motions, forces and mode transitions in vortex-induced vibrations at low mass-damping. *Journal of Fluids and Structures*, **13**, (1999), 813-853.
7. HAYASHI, K., TANAKA, K., FUJIMA, K. AND SHIGEMURA, T.: Fluid Force Acting on a Vortex Excited Circular Cylinder Vibrating in Steady Flow, National Defense Academy Science and Engineering Research Report, 34(2), (1997), 11-23. (in Japanese)